Int J Mech Mater Des (2017) 13:481–497
DOI 10.1007/s10999-016-9354-1

Dynamic behavior of micro-resonator under alternating current voltage

X. Chen · S. A. Meguid

Received: 15 July 2016 / Accepted: 19 September 2016 / Published online: 22 September 2016

Abstract This paper investigates the dynamic behavior of a micro-resonator under various levels of Alternating Current (AC) voltage, without a biased Direct Current voltage. The governing equations are developed in the framework of Euler–Bernoulli beam theory, accounting for the effects of damping, fringing field, and mid-plane stretching using von Karman nonlinear strain. The steady-state frequency response of the micro-resonator is derived from the governing equations by the method of multiple scales. The transient response is also derived by the long-time integration. The results of our work reveal that the applied AC voltage and the mid-plane stretching (quantified by a stretching parameter) determine the characteristic feature of the dynamic behavior of the micro-resonator, such as the dynamic pull-in, the frequency response of linear or hardening characteristic. A design diagram in terms of AC voltage amplitude and stretching parameter is developed to show the domains of the different dynamic behavior characteristics. Our results also reveal the significant effects of damping and boundary conditions on the dynamic behavior and the design diagram of the micro-resonator.

X. Chen · S. A. Meguid (✉)
Mechanics and Aerospace Design Laboratory,
Department of Mechanical and Industrial Engineering,
University of Toronto, 5 King's College Road, Toronto,
ON M5S 3G8, Canada
e-mail: meguid@mie.utoronto.ca

Keywords Micro-resonator · Frequency response · Dynamic pull-in · Design diagram · Mid-plane stretching · Boundary conditions

1 Introduction

The Micro/Nano-Electro-Mechanical Systems (MEMS/NEMS) have various unique advantages such as small size, high precision and low power consumption. Among MEMS/NEMS, the micro/nanobeam system is one of the most studied in the literature, and the applications such as switches and non-volatile memories have been found in these systems (Brown 1998; Charlot et al. 2008; Intaraprasonk and Fan 2011; Jang et al. 2008; Roodenburg et al. 2009; Rueckes et al. 2000). The micro/-nanobeams can also be driven to vibration by an Alternating Current (AC) voltage, and the obtained micro/nano-resonators can be used as mass sensors, temperature sensors, transmitters and receivers (Burg et al. 2007; Chaste et al. 2012; Chiu et al. 2008; Eltaher et al. 2016; Hopcroft et al. 2007; Kivi et al. 2015; Kwon et al. 2008; Mohanty 2005; Peng et al. 2006; Southworth et al. 2010; Wang and Arash 2014; Yang et al. 2006).

Theoretical and experimental studies on the primary resonance frequency of the micro/nano-resonator have been conducted in the literature, and the evolutions of resonance frequency with the applied AC voltage and a biased DC (direct current) voltage have been largely reported (Jia et al. 2012; Jonsson et al. 2004; Kuang and Chen 2004; Tilmans and Legtenberg 1994). The dynamic behavior of the micro/nano-resonator have also been reported, and the frequency response curves of linear, hardening, and softening characteristics have been observed in the experiments (Almog et al. 2007; Alsaleem et al. 2009; Badzey et al. 2004; Carr et al. 1999; Evoy et al. 1999; Mestrom et al. 2008; Ruzziconi et al. 2013; Tilmans and Legtenberg 1994; Zook et al. 1992) as well as predicted from the theoretical investigations (Caruntu and Knecht 2011; Caruntu et al. 2013; Caruntu and Martinez 2014; Farokhi and Ghayesh 2015a, b; Gui et al. 1998; Kacem et al. 2011; Kim and Lee 2013; Ouakad and Younis 2010; Rhoads et al. 2006; Ruzziconi et al. 2013).

Careful literature review indicates that most of the work is concerned with the micro/nano-resonator biased by a DC voltage. Caruntu and Knecht (2011), Caruntu et al. (2013), and Caruntu and Martinez (2014) studied theoretically a non-biased cantilever-type micro-resonator, and the dynamic pull-in near the primary resonance regime was found. Moreover, most work is conducted at a certain level of the applied voltages, and one characteristic feature of the dynamic behavior is observed or predicted. Studies concerned with characterizing the dynamic behavior of the micro/-nano-resonator at different levels of the applied voltages and determining the parameters which govern the dynamic behavior characteristics are limited.

In this paper, we extend the earlier work to study the dynamic behavior of the non-biased micro-resonator at different levels of AC voltage. The remaining parts of the paper are organized as follows. Section 2 is devoted to the beam model formulation. In Sect. 3, the methods of multiple scales and long-time integration are presented to obtain respectively the steady-state frequency response and the transient response of the microbeam from the beam model. Various effects on the dynamic behavior of the microbeam are investigated in Sect. 4, including the effects of mid-plane stretching, fringing field, damping, and boundary conditions. A design diagram in terms of AC voltage amplitude and mid-plane stretching parameter is also developed, indicating the domains of different characteristic features of the dynamic behavior. Finally, a general conclusion is given in Sect. 5.

2 Model formulation

The situation envisaged is that of an electrically actuated rectangular microbeam of length L, width b and thickness h, as depicted in Fig. 1. Suppose that the displacements u_x, u_y and u_z of any point in the beam only depend on x- and z-coordinate, and u_y is equal to 0, i.e., no displacement along y-coordinate. Further suppose that the studied microbeam is thin ($h \ll L$), then the Euler–Bernoulli beam theory can be applied as:

$$u_x(x,z,t) = u(x,t) - z\frac{\partial w}{\partial x}(x,t) \tag{1a}$$

$$u_z(x,z,t) = w(x,t) \tag{1b}$$

where t is time, u and w are respectively the axial (along x-coordinate) and transverse (along z) displacements of a point on the mid-plane of the beam. The von Karman nonlinear strain is used to account for the geometric nonlinearity due to mid-plane stretching. Therefore, the only nonzero strain component from Eq. (1) is (Reddy 2011):

$$\varepsilon_{xx} = \frac{\partial u_x}{\partial x} + \frac{1}{2}\left(\frac{\partial u_z}{\partial x}\right)^2 = \frac{\partial u}{\partial x} - z\frac{\partial^2 w}{\partial x^2} + \frac{1}{2}\left(\frac{\partial w}{\partial x}\right)^2 \tag{2}$$

Considering Eq. (2), we calculate the variation δU_{elas} of the elastic strain energy as:

$$\begin{aligned}\delta U_{elas} &= \int_0^L \int_S \left(\underline{\underline{\sigma}} : \delta\underline{\underline{\varepsilon}}\right) ds\,dx \\ &= -\int_0^L \frac{\partial N(x,t)}{\partial x}\delta u\,dx \\ &\quad - \int_0^L \left(\frac{\partial^2 M(x,t)}{\partial x^2} + \frac{\partial}{\partial x}\left(N(x,t)\frac{\partial w}{\partial x}\right)\right)\delta w\,dx \\ &\quad + N(x,t)\delta u\big|_{x=0}^{L} + \left(\frac{\partial M(x,t)}{\partial x} + N(x,t)\frac{\partial w}{\partial x}\right) \\ &\quad \delta w\bigg|_{x=0}^{L} - M(x,t)\frac{\partial \delta w}{\partial x}\bigg|_{x=0}^{L}\end{aligned} \tag{3}$$

where $\int_S ds$ is the integral over the cross section, i.e., the y–z plane in Fig. 1; the axial force N and the bending moment M are defined as follows:

$$N = \int_S \sigma_{xx} ds \tag{4a}$$

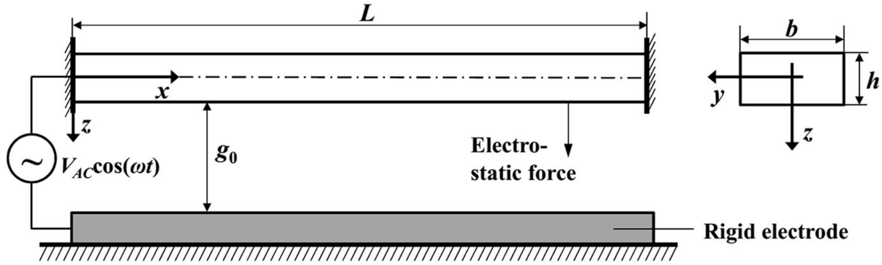

Fig. 1 Clamped–clamped microbeam actuated by alternating current voltage. The *arrow* indicates the direction of the induced distributed electrostatic force

$$M = \int_S z\sigma_{xx} ds \tag{4b}$$

The variation δE_k of the kinetic energy is calculated with the aid of Eq. (1) as:

$$\delta E_k = \int_0^L \int_S \rho \left(\frac{\partial u_x}{\partial t} \frac{\partial \delta u_x}{\partial t} + \frac{\partial u_z}{\partial t} \frac{\partial \delta u_z}{\partial t} \right) ds\, dx$$
$$= \int_0^L \left(\rho S \left(\frac{\partial u}{\partial t} \frac{\partial \delta u}{\partial t} + \frac{\partial w}{\partial t} \frac{\partial \delta w}{\partial t} \right) + \rho I \left(\frac{\partial^2 w}{\partial x \partial t} \frac{\partial^2 \delta w}{\partial x \partial t} \right) \right) dx \tag{5}$$

where ρ is the mass density, S (=bh) is the cross-sectional area, and I (=$bh^3/12$) is the second moment of area.

The variation δW_{ext} of the work done by the external forces is:

$$\delta W_{ext} = \int_0^L \left(f_{damp} + f_{elec} \right) \delta w\, dx \tag{6}$$

where f_{damp} and f_{elec} are respectively the viscous damping force and the electrostatic force per unit length. We can estimate f_{damp} as:

$$f_{damp} = -c_d \frac{\partial w}{\partial t} \tag{7}$$

with c_d being the damping coefficient per unit length. Considering a small gap ($\ll$ beam length) between the beam and the electrode, we can regard the beam and the electrode as a parallel-plate capacitor. To further consider the fringing fields at the edges of the microbeam, Palmer's formula (Palmer 1937) is used, and the electrostatic force f_{elec} is calculated as (Caruntu and Knecht 2011; Gupta 1997):

$$f_{elec} = \frac{1}{2} \frac{\varepsilon_0 b (V_{AC} \cos(\omega t))^2}{(g_0 - w)^2} \left(1 + 0.65 \frac{g_0 - w}{b} \right) \tag{8}$$

where ε_0 (=8.8542×10^{-12} F $\cdot$ m^{-1}) is the vacuum permittivity, b is the beam width, g_0 is the initial gap between the beam and the rigid electrode, as shown in Fig. 1, and V_{AC} is the amplitude of the applied AC voltage with the angular velocity ω. It is noted that Palmer's formula is only valid for wide microbeams, i.e., $b > 5\,h$ and $b > 10 g_0$ (Caruntu and Knecht 2011). When the beam is narrow, more complicated formulae such as (Batra et al. 2006; van der Meijs and Fokkema 1984) should be used.

Introducing Eqs. (3), (5) and (6) into the following Hamilton's principle

$$\int_0^{t_1} \left(\delta E_k + \delta W_{ext} - \delta U_{elas} \right) dt = 0 \tag{9}$$

and integrating the result by parts with respect to t and x, we arrive at:

$$\int_0^{t_1} \int_0^L \left(\frac{\partial N}{\partial x} - \rho S \frac{\partial^2 u}{\partial t^2} \right) \delta u dx dt$$
$$+ \int_0^{t_1} \int_0^L \left(\frac{\partial^2 M}{\partial x^2} + \frac{\partial}{\partial x} \left(N \frac{\partial w}{\partial x} \right) + f_{damp} + f_{elec} \right.$$
$$\left. - \rho S \frac{\partial^2 w}{\partial t^2} + \rho I \frac{\partial^4 w}{\partial x^2 \partial t^2} \right) \delta w dx dt + \int_0^{t_1}$$
$$\times \left(-N \delta u - \left(\frac{\partial M}{\partial x} + N \frac{\partial w}{\partial x} + \rho I \frac{\partial^3 w}{\partial x \partial t^2} \right) \delta w M \frac{\partial \delta w}{\partial x} \right) \Bigg|_{x=0}^{L} dt$$
$$+ \int_0^L \left(\rho S \frac{\partial u}{\partial t} \delta u + \rho S \frac{\partial w}{\partial t} \delta w + \rho I \frac{\partial^2 w}{\partial x \partial t} \frac{\partial \delta w}{\partial x} \right) \Bigg|_{t=0}^{t_1} dx = 0 \tag{10}$$

The following governing equations can be obtained from Eqs. (7), (8) and (10):

$$\delta u : \frac{\partial N}{\partial x} - \rho S \frac{\partial^2 u}{\partial t^2} = 0 \tag{11a}$$

$$\delta w : \frac{\partial^2 M}{\partial x^2} + \frac{\partial}{\partial x} \left(N \frac{\partial w}{\partial x} \right) - \rho S \frac{\partial^2 w}{\partial t^2} + \rho I \frac{\partial^4 w}{\partial x^2 \partial t^2}$$
$$- c_d \frac{\partial w}{\partial t} + \frac{1}{2} \frac{\varepsilon_0 b (V_{AC} \cos(\omega t))^2}{(g_0 - w)^2} \left(1 + 0.65 \frac{g_0 - w}{b} \right)$$
$$= 0 \tag{11b}$$

Since the studied microbeam is thin (thickness $\ll$ length), the axial displacement u and the beam curvature $\frac{\partial^2 w}{\partial x^2}$ are quite small and negligible with respect to the transverse displacement w. As a result, we neglect the axial inertia term $\rho S \frac{\partial^2 u}{\partial t^2}$ and the rotational inertia term $\rho I \frac{\partial^4 w}{\partial x^2 \partial t^2}$ in Eq. (11), and obtain:

$$\delta u : \frac{\partial N}{\partial x} = 0 \tag{12a}$$

$$\delta w : \frac{\partial^2 M}{\partial x^2} + \frac{\partial}{\partial x}\left(N\frac{\partial w}{\partial x}\right) - \rho S\frac{\partial^2 w}{\partial t^2} - c_d\frac{\partial w}{\partial t} + \frac{1}{2}\frac{\varepsilon_0 b (V_{AC}\cos(\omega t))^2}{(g_0 - w)^2}\left(1 + 0.65\frac{g_0 - w}{b}\right) = 0 \tag{12b}$$

with Eqs. (12a), (12b) can be reduced to:

$$\frac{\partial^2 M}{\partial x^2} + N\frac{\partial^2 w}{\partial x^2} - \rho S\frac{\partial^2 w}{\partial t^2} - c_d\frac{\partial w}{\partial t} + \frac{1}{2}\frac{\varepsilon_0 b (V_{AC}\cos(\omega t))^2}{(g_0 - w)^2}\left(1 + 0.65\frac{g_0 - w}{b}\right) = 0 \tag{13}$$

Suppose that the beam material is elastically isotropic with Young's modulus E and Poisson's ratio v. Then the 1D constitutive relation becomes:

$$\sigma_{xx} = E^* \varepsilon_{xx} \tag{14}$$

where E^* is the effective Young's modulus. We take $E^* = E/(1 - v^2)$ for the wide microbeam studied here. When the beam is narrow, $E^* = E$. Introducing Eqs. (2) and (14) into Eq. (4), we have:

$$N = E^* S\left(\frac{\partial u}{\partial x} + \frac{1}{2}\left(\frac{\partial w}{\partial x}\right)^2\right) \tag{15a}$$

$$M = -E^* I\frac{\partial^2 w}{\partial x^2} \tag{15b}$$

Equation (12a) shows that the axial force N is constant along x-coordinate. Using Eq. (15a), we estimate N as the following average value:

$$N = \frac{E^* S}{2L}\left(\int_0^L \left(\frac{\partial w}{\partial x}\right)^2 dx\right) \tag{16}$$

To obtain Eq. (16), we have used the boundary conditions of clamped–clamped beam, i.e., $u(0) = u(L) = 0$. Introducing Eqs. (15b) and (16) into Eq. (13), we obtain:

$$\rho S\frac{\partial^2 w}{\partial t^2} + c_d\frac{\partial w}{\partial t} + E^* I\frac{\partial^4 w}{\partial x^4} - \frac{E^* S}{2L}\left(\int_0^L \left(\frac{\partial w}{\partial x}\right)^2 dx\right)\frac{\partial^2 w}{\partial x^2} = \frac{1}{2}\frac{\varepsilon_0 b (V_{AC}\cos(\omega t))^2}{(g_0 - w)^2}\left(1 + 0.65\frac{g_0 - w}{b}\right) \tag{17}$$

Considering the dimensionless quantities in Table 1, we rewrite Eq. (17) in the following dimensionless form:

$$\frac{\partial^2 \overline{w}}{\partial \overline{t}^2} + \overline{c_d}\frac{\partial \overline{w}}{\partial \overline{t}} + \frac{\partial^4 \overline{w}}{\partial \overline{x}^4} - \alpha\left(\int_0^1 \left(\frac{\partial \overline{w}}{\partial \overline{x}}\right)^2 d\overline{x}\right)\frac{\partial^2 \overline{w}}{\partial \overline{x}^2} = \left(\overline{V_{AC}}\cos(\overline{\omega}\overline{t})\right)^2\left(\frac{1}{(1 - \overline{w})^2} + \frac{\beta}{(1 - \overline{w})}\right) \tag{18}$$

In Eq. (18), the 4th term on the left-hand-side with a stretching parameter α represents the effect of mid-plane stretching, which stiffens the microbeam. The dimensionless boundary conditions of the clamped–clamped microbeam are:

$$\delta\overline{w} : \overline{w}(0, \overline{t}) = 0, \quad \overline{w}(1, \overline{t}) = 0 \tag{19a}$$

$$\frac{\partial \delta\overline{w}}{\partial \overline{x}} : \frac{\partial \overline{w}}{\partial \overline{x}}(0, \overline{t}) = 0, \quad \frac{\partial \overline{w}}{\partial \overline{x}}(1, \overline{t}) = 0 \tag{19b}$$

3 Solution methodology

3.1 Method of multiple scales

The micro-resonator is usually vibrating at low amplitude with small damping effect. In this case, the method of multiple scales can be used (Caruntu and Knecht 2011; Ouakad and Younis 2010). Considering low vibration amplitude, small damping, and weak nonlinearity, we expand the electrostatic force around $\overline{w} = 0$ in Eq. (18), and further set the electrostatic force, damping and mid-plane stretching terms to a slow scale by multiplying them by a small bookkeeping parameter ξ:

$$\frac{\partial^2 \overline{w}}{\partial \overline{t}^2} + \xi\overline{c_d}\frac{\partial \overline{w}}{\partial \overline{t}} + \frac{\partial^4 \overline{w}}{\partial \overline{x}^4} - \xi\alpha\left(\int_0^1 \left(\frac{\partial \overline{w}}{\partial \overline{x}}\right)^2 d\overline{x}\right)\frac{\partial^2 \overline{w}}{\partial \overline{x}^2} = \xi\left(\overline{V_{AC}}\cos(\overline{\omega}\overline{t})\right)^2\left(1 + \beta + (2 + \beta)\overline{w} + (3 + \beta)\overline{w}^2 + (4 + \beta)\overline{w}^3\right) \tag{20}$$

Introducing the first-order expansion of the dimensionless deflection $\overline{w}$ as:

Table 1 Dimensionless quantities adopted in the study

Quantity	Expression	Meaning
$\overline{c_d}$	$c_d L^2/\sqrt{E^* I \rho S}$	Dimensionless damping coefficient
$\bar{t}$	$t/\sqrt{\rho S L^4/(E^* I)}$	Dimensionless time
$\overline{V_{AC}}$	$V_{AC}/\sqrt{E^* h^3 g_0^3/(6\varepsilon_0 L^4)}$	Dimensionless AC voltage amplitude
$\overline{w}$	w/g_0	Dimensionless deflection
$\overline{x}$	x/L	Normalized coordinate
α	$6(g_0/h)^2$	Stretching parameter
β	$0.65(g_0/b)$	Fringing field parameter
$\overline{\omega}$	$\omega/\sqrt{E^* I/(\rho S L^4)}$	Dimensionless angular frequency

$$\overline{w} = \overline{w}_0(\overline{x}, T_0, T_1) + \xi \overline{w}_1(\overline{x}, T_0, T_1) \tag{21}$$

with T_0 (=$\bar{t}$) being the fast time scale and T_1 (=$\xi\bar{t}$) being the slow time scale, we derive the following time derivatives from Eq. (21):

$$\frac{\partial \overline{w}}{\partial \bar{t}} = \frac{\partial \overline{w}_0}{\partial T_0} + \left(\frac{\partial \overline{w}_0}{\partial T_1} + \frac{\partial \overline{w}_1}{\partial T_0}\right)\xi + \frac{\partial \overline{w}_1}{\partial T_1}\xi^2 \tag{22a}$$

$$\frac{\partial^2 \overline{w}}{\partial \bar{t}^2} = \frac{\partial^2 \overline{w}_0}{\partial T_0^2} + \left(2\frac{\partial^2 \overline{w}_0}{\partial T_0 \partial T_1} + \frac{\partial^2 \overline{w}_1}{\partial T_0^2}\right)\xi + \left(\frac{\partial^2 \overline{w}_0}{\partial T_1^2} + 2\frac{\partial^2 \overline{w}_1}{\partial T_0 \partial T_1}\right)\xi^2 + \frac{\partial^2 \overline{w}_1}{\partial T_1^2}\xi^3 \tag{22b}$$

By introducing Eqs. (21) and (22) into Eqs. (19) and (20), and equating the like powers of ξ, we obtain:

Order ξ^0:

$$\frac{\partial^2 \overline{w}_0}{\partial T_0^2} + \frac{\partial^4 \overline{w}_0}{\partial \overline{x}^4} = 0 \tag{23a}$$

$$\overline{w}_0(0, T_0, T_1) = 0,\ \overline{w}_0(1, T_0, T_1) = 0,\ \frac{\partial \overline{w}_0}{\partial \overline{x}}(0, T_0, T_1) = 0,\ \frac{\partial \overline{w}_0}{\partial \overline{x}}(1, T_0, T_1) = 0 \tag{23b}$$

Order ξ^1:

$$\frac{\partial^2 \overline{w}_1}{\partial T_0^2} + \frac{\partial^4 \overline{w}_1}{\partial \overline{x}^4} = -2\frac{\partial^2 \overline{w}_0}{\partial T_0 \partial T_1} - \overline{c_d}\frac{\partial \overline{w}_0}{\partial T_0} + \alpha\left(\int_0^1 \left(\frac{\partial \overline{w}_0}{\partial \overline{x}}\right)^2 d\overline{x}\right)\frac{\partial^2 \overline{w}_0}{\partial \overline{x}^2} + \left(\overline{V_{AC}}\cos(\overline{\omega} T_0)\right)^2 \left(1 + \beta + (2+\beta)\overline{w}_0 + (3+\beta)\overline{w}_0^2 + (4+\beta)\overline{w}_0^3\right) \tag{24a}$$

$$\overline{w}_1(0, T_0, T_1) = 0,\ \overline{w}_1(1, T_0, T_1) = 0,\ \frac{\partial \overline{w}_1}{\partial \overline{x}}(0, T_0, T_1) = 0,\ \frac{\partial \overline{w}_1}{\partial \overline{x}}(1, T_0, T_1) = 0 \tag{24b}$$

Suppose that the solution to Eq. (23) is:

$$\overline{w}_0 = \phi_j(\overline{x})\left(A(T_1)e^{i\omega_j T_0} + A^*(T_1)e^{-i\omega_j T_0}\right) \tag{25}$$

where A is a coefficient depending on the slow time scale T_1 and A^* is its complex conjugate; ϕ_j ($j = 1, 2, \ldots, n$) is the jth linear undamped vibration mode of the clamped–clamped beam, being:

$$\phi_j(\overline{x}) = C_j\left(\cosh(\lambda_j \overline{x}) - \cos(\lambda_j \overline{x}) - \frac{\sinh(\lambda_j) + \sin(\lambda_j)}{\cosh(\lambda_j) - \cos(\lambda_j)}\left(\sinh(\lambda_j \overline{x}) - \sin(\lambda_j \overline{x})\right)\right) \tag{26}$$

where C_j is a constant satisfying $\max_{\overline{x}\in[0,1]}\left|\phi_j(\overline{x})\right| = 1$, and λ_j is a frequency parameter satisfying $\cosh(\lambda_j)\cos(\lambda_j) = 1$. λ_j is related to the resonance angular frequency ω_j by: $\omega_j = \lambda_j^2$. The micro-resonator usually works near the primary resonance regime, so we only consider the first vibration mode here, i.e., $j = 1$ in Eq. (25). The square of the applied voltage can be expressed as:

$$\left(\overline{V_{AC}}\cos(\varpi T_0)\right)^2 = \frac{1}{2}\overline{V_{AC}}^2 + \frac{1}{2}\overline{V_{AC}}^2\cos(2\varpi T_0) \tag{27}$$

Equation (27) shows that the microbeam vibrates at a frequency of 2ϖ. To indicate the nearness of 2ϖ to the primary resonance frequency ω_1, a detuning parameter δ is introduced as:

$$2\varpi = \omega_1 + \xi\delta \tag{28}$$

with Eqs. (28), (27) can be rewritten as:

$$\left(\overline{V_{AC}}\cos(\varpi T_0)\right)^2 = \frac{1}{2}\overline{V_{AC}}^2 + \frac{1}{4}\overline{V_{AC}}^2\left(e^{i(\omega_1 T_0 + T_1\delta)} + e^{-i(\omega_1 T_0 + T_1\delta)}\right) \tag{29}$$

By introducing Eqs. (25) and (29) into the right-hand-side of Eq. (24a), we have:

$$\begin{aligned}\frac{\partial^2 \overline{w}_1}{\partial T_0^2} + \frac{\partial^4 \overline{w}_1}{\partial \overline{x}^4} = {} & c_0 + \left(c_1 e^{i\omega_1 T_0} + c_1^* e^{-i\omega_1 T_0}\right) \\ & + \left(c_2 e^{i(2\omega_1 T_0)} + c_2^* e^{-i(2\omega_1 T_0)}\right) \\ & + \left(c_3 e^{i(3\omega_1 T_0)} + c_3^* e^{-i(3\omega_1 T_0)}\right) \\ & + \left(c_4 e^{i(4\omega_1 T_0)} + c_4^* e^{-i(4\omega_1 T_0)}\right)\end{aligned} \tag{30}$$

with $c_0 \sim c_4$ being coefficients and $c_1^* \sim c_4^*$ being the complex conjugates of $c_1 \sim c_4$. c_1 is calculated as:

$$\begin{aligned}c_1 = {} & -2i\omega_1\phi_1\frac{dA}{dT_1} - i\overline{c_d}\omega_1\phi_1 A \\ & + 3\alpha\phi_1''\left(\int_0^1 (\phi_1'')^2 d\overline{x}\right)A^2A^* + \frac{1}{2}(2+\beta)\overline{V_{AC}}^2\phi_1 A \\ & + \frac{3}{2}(4+\beta)\overline{V_{AC}}^2\phi_1^3 A^2A^* + \frac{1}{4}(1+\beta)\overline{V_{AC}}^2 e^{iT_1\delta} \\ & + \frac{1}{2}(3+\beta)\overline{V_{AC}}^2\phi_1^2 AA^* e^{iT_1\delta} \\ & + \frac{1}{4}(3+\beta)\overline{V_{AC}}^2\phi_1^2 A^2 e^{-iT_1\delta}\end{aligned} \tag{31}$$

where a superimposed apostrophe denotes a derivative with respect to the normalized coordinate $\overline{x}$. The solvability condition states that the right-hand-side of Eq. (30) must be orthogonal to any solution of Eq. (23), which is expressed in Eq. (25) with $j = 1$ (Caruntu and Knecht 2011). Then we have:

$$c_1\phi_1 = 0 \tag{32}$$

Introducing Eq. (31) into Eq. (32) and integrating the result from $\overline{x} = 0$ to 1, we obtain:

$$\begin{aligned} & -2i\omega_1 m_2\frac{dA}{dT_1} - i\overline{c_d}\omega_1 m_2 A + 3\alpha s_1 A^2A^* \\ & + \frac{1}{2}(2+\beta)\overline{V_{AC}}^2 m_2 A + \frac{3}{2}(4+\beta)\overline{V_{AC}}^2 m_4 A^2A^* \\ & + \frac{1}{4}(1+\beta)\overline{V_{AC}}^2 m_1 e^{iT_1\delta} + \frac{1}{2}(3+\beta)\overline{V_{AC}}^2 m_3 AA^* e^{iT_1\delta} \\ & + \frac{1}{4}(3+\beta)\overline{V_{AC}}^2 m_3 A^2 e^{-iT_1\delta} = 0\end{aligned} \tag{33}$$

where the parameters are given below:

$$\begin{aligned} & m_1 = \int_0^1 \phi_1 d\overline{x},\ m_2 = \int_0^1 \phi_1^2 d\overline{x},\ m_3 \\ & = \int_0^1 \phi_1^3 d\overline{x},\ m_4 = \int_0^1 \phi_1^4 d\overline{x} \\ & s_1 = \left(\int_0^1 (\phi_1')^2 d\overline{x}\right)\left(\int_0^1 \phi_1\phi_1'' d\overline{x}\right)\end{aligned} \tag{34}$$

Express $A(T_1)$ in the following polar form:

$$A(T_1) = \frac{1}{2}a(T_1)e^{i\theta(T_1)} \tag{35}$$

It can be derived from Eqs. (25) and (35) that a is the vibration amplitude. The time derivative can be obtained from Eq. (35) as:

$$\frac{dA}{dT_1} = \frac{1}{2}\left(\frac{da}{dT_1}e^{i\theta} + a\frac{d\theta}{dT_1}ie^{i\theta}\right) \tag{36}$$

Introducing Eqs. (35) and (36) into Eq. (33), separating the real and imaginary parts, and after several calculations we obtain:

$$\begin{aligned}\frac{da}{dT_1} = {} & -\frac{\overline{c_d}}{2}a + \left(\frac{m_1}{4m_2\omega_1}(1+\beta) + \frac{m_3}{16m_2\omega_1}(3+\beta)a^2\right) \\ & \times \overline{V_{AC}}^2\sin(T_1\delta - \theta)\end{aligned} \tag{37a}$$

$$\begin{aligned}a\frac{d\theta}{dT_1} = {} & -\frac{1}{4\omega_1}(2+\beta)\overline{V_{AC}}^2 a - \frac{3\alpha s_1}{8m_2\omega_1}a^3 \\ & - \frac{3m_4}{16m_2\omega_1}(4+\beta)\overline{V_{AC}}^2 a^3 \\ & - \left(\frac{m_1}{4m_2\omega_1}(1+\beta) + \frac{3m_3}{16m_2\omega_1}(3+\beta)a^2\right) \\ & \times \overline{V_{AC}}^2\cos(T_1\delta - \theta)\end{aligned} \tag{37b}$$

With the phase lag γ:

$$\gamma = T_1\delta - \theta \tag{38}$$

Equation (37) can be rewritten as:

$$\frac{da}{dT_1} = -\frac{\overline{c_d}}{2}a + \left(\frac{m_1}{4m_2\omega_1}(1+\beta) + \frac{m_3}{16m_2\omega_1}(3+\beta)a^2\right)\overline{V_{AC}}^2 \sin\gamma \tag{39a}$$

$$a\frac{d\gamma}{dT_1} = a\delta + \frac{1}{4\omega_1}(2+\beta)\overline{V_{AC}}^2 a + \frac{3\alpha s_1}{8m_2\omega_1}a^3 + \frac{3m_4}{16m_2\omega_1}(4+\beta)\overline{V_{AC}}^2 a^3 + \left(\frac{m_1}{4m_2\omega_1}(1+\beta) + \frac{3m_3}{16m_2\omega_1}(3+\beta)a^2\right) \times \overline{V_{AC}}^2 \cos\gamma \tag{39b}$$

When the response of the microbeam becomes steady, we have $\frac{da}{dT_1} = 0$ and $\frac{d\gamma}{dT_1} = 0$. In this case, Eq. (39) can be reduced to:

$$\left(\frac{m_1}{4m_2\omega_1}(1+\beta) + \frac{m_3}{16m_2\omega_1}(3+\beta)a^2\right)\overline{V_{AC}}^2 \sin\gamma = \frac{\overline{c_d}}{2}a \tag{40a}$$

$$\left(\frac{m_1}{4m_2\omega_1}(1+\beta) + \frac{3m_3}{16m_2\omega_1}(3+\beta)a^2\right)\overline{V_{AC}}^2 \cos\gamma = -a\delta - \frac{1}{4\omega_1}(2+\beta)\overline{V_{AC}}^2 a - \frac{3\alpha s_1}{8m_2\omega_1}a^3 - \frac{3m_4}{16m_2\omega_1}(4+\beta)\overline{V_{AC}}^2 a^3 \tag{40b}$$

Combining Eqs. (40a) and (40b), we have:

$$b_1^2 b_3^2 a^{10} + \left(2b_1^2 b_3 b_4 + 2b_1 b_2 b_3^2 - 9b_1^4 b_6^2\right)a^8 + \left(b_1^2 b_4^2 + 4b_1 b_2 b_3 b_4 + b_2^2 b_3^2 + 9b_1^2 b_5^2 - 24 b_1^3 b_2 b_6^2\right)a^6 + \left(2b_1 b_2 b_4^2 + 2b_2^2 b_3 b_4 + 6b_1 b_2 b_5^2 - 22 b_1^2 b_2^2 b_6^2\right)a^4 + \left(b_2^2 b_4^2 + b_2^2 b_5^2 - 8b_1 b_2^3 b_6^2\right)a^2 - b_2^4 b_6^2 = 0 \tag{41a}$$

$$\gamma = arccos\left(-\frac{(b_4 a + b_3 a^3)}{b_6(b_2 + 3b_1 a^2)}\right) \tag{41b}$$

where the coefficients $b_1 \sim b_6$ are:

$$b_1 = \frac{m_3}{16m_2\omega_1}(3+\beta),\ b_2 = \frac{m_1}{4m_2\omega_1}(1+\beta),$$
$$b_3 = \frac{3\alpha s_1}{8m_2\omega_1} + \frac{3m_4}{16m_2\omega_1}(4+\beta)\overline{V_{AC}}^2$$
$$b_4 = \delta + \frac{1}{4\omega_1}(2+\beta)\overline{V_{AC}}^2,\ b_5 = \frac{\overline{c_d}}{2},\ b_6 = \overline{V_{AC}}^2 \tag{42}$$

To study the damping effect, a quality factor Q is commonly used, which is related to the dimensionless damping coefficient $\overline{c_d}$ by (Nayfeh et al. 2007):

$$\overline{c_d} = \frac{\omega_1}{Q} \tag{43}$$

By solving Eq. (41a) at different levels of the detuning parameter δ, we can obtain the steady-state frequency response of the microbeam, i.e., the evolution of the maximum deflection (normalized as the dimensionless vibration amplitude a) with the applied angular frequency (normalized as $\overline{\omega}$, calculated from Eq. (28) with $\xi = 1$).

To analyze the stability of each point (δ_0, a_0) on the frequency response curve, we take the following procedures: by introducing $\delta = \delta_0$ and $a = a_0$ into Eq. (41b) and solving the resulting equation, we obtain the phase lag γ_0; further introducing γ_0 and a_0 into the following Jacobian matrix J_a of Eq. (39):

$$J_a = \begin{bmatrix} \frac{\partial(da/dT_1)}{\partial a} & \frac{\partial(da/dT_1)}{\partial \gamma} \\ \frac{\partial(d\gamma/dT_1)}{\partial a} & \frac{\partial(d\gamma/dT_1)}{\partial \gamma} \end{bmatrix} = \begin{bmatrix} -b_5 + 2b_1 b_6 a \sin\gamma & (b_2 + b_1 a^2) b_6 \cos\gamma \\ 2b_3 a - \left(\frac{b_2}{a^2} - 3b_1\right) b_6 \cos\gamma & -\left(\frac{b_2}{a} + 3b_1 a\right) b_6 \sin\gamma \end{bmatrix} \tag{44}$$

we calculate the eigenvalues of J_a. If the real parts of all the eigenvalues are negative, the point (δ_0, a_0) is stable; otherwise, it is unstable.

3.2 Long-time integration

To validate the steady-state frequency response obtained from the analytical model given in Eq. (41a), we solve the governing equation Eq. (18) with the boundary conditions of Eq. (19) to obtain the time evolution of the beam deflection at each frequency. To do so, the Galerkin decomposition of the dimensionless deflection $\overline{w}$ is used (Jia et al. 2012; Kim and Lee 2013; Ouakad and Younis 2010; Rhoads et al. 2006; Ruzziconi et al. 2013):

$$\overline{w}=\sum_{j=1}^{n}q_j(\overline{t})\phi_j(\overline{x}) \tag{45}$$

where ϕ_j ($j=1, 2, \ldots, n$) is the jth linear undamped vibration mode of the straight clamped–clamped beam, which has already been given in Eq. (26), and q_j is its generalized coordinate. Multiplying Eq. (18) by $(1-\overline{w})^2$, introducing Eq. (45), and further multiplying the result by ϕ_i ($i=1, 2, \ldots, n$) and integrating from $\overline{x}=0$ to 1, we obtain the following n-degree-of-freedom reduced-order model:

$$\begin{aligned}
&\left(\int_0^1 \phi_i^2 d\overline{x}\right)\ddot{q}_i-2\sum_{j=1}^{n}\sum_{k=1}^{n}\left(\int_0^1 \phi_k\phi_j\phi_i\,d\overline{x}\right)q_k\ddot{q}_j\\
&+\sum_{j=1}^{n}\sum_{k=1}^{n}\sum_{l=1}^{n}\left(\int_0^1 \phi_l\phi_k\phi_j\phi_i\,d\overline{x}\right)q_lq_k\ddot{q}_j\\
&+\overline{c_d}\left(\int_0^1 \phi_i^2 d\overline{x}\right)\dot{q}_i-2\overline{c_d}\sum_{j=1}^{n}\sum_{k=1}^{n}\left(\int_0^1 \phi_k\phi_j\phi_i\,d\overline{x}\right)q_k\dot{q}_j\\
&+\overline{c_d}\sum_{j=1}^{n}\sum_{k=1}^{n}\sum_{l=1}^{n}\left(\int_0^1 \phi_l\phi_k\phi_j\phi_i\,d\overline{x}\right)q_lq_k\dot{q}_j\\
&+\lambda_i^4\left(\int_0^1 \phi_i^2 d\overline{x}\right)q_i-2\sum_{j=1}^{n}\sum_{k=1}^{n}\left(\int_0^1 \phi_k\phi_j\phi_i\,d\overline{x}\right)\lambda_j^4q_kq_j\\
&+\sum_{j=1}^{n}\sum_{k=1}^{n}\sum_{l=1}^{n}\left(\int_0^1 \phi_l\phi_k\phi_j\phi_i\,d\overline{x}\right)\lambda_j^4q_lq_kq_j\\
&-\alpha\left(\sum_{j=1}^{n}\sum_{k=1}^{n}\left(\int_0^1 \phi_k'\phi_j' d\overline{x}\right)q_kq_j\right)\left(\sum_{j=1}^{n}\left(\int_0^1 \phi_j''\phi_i\,d\overline{x}\right)q_j\right.\\
&-2\sum_{j=1}^{n}\sum_{k=1}^{n}\left(\int_0^1 \phi_k\phi_j''\phi_i\,d\overline{x}\right)q_kq_j\\
&\left.+\sum_{j=1}^{n}\sum_{k=1}^{n}\sum_{l=1}^{n}\left(\int_0^1 \phi_l\phi_k\phi_j''\phi_i\,d\overline{x}\right)q_lq_kq_j\right)\\
&=\left(\overline{V_{AC}}\cos(\overline{\omega}\overline{t})\right)^2\left((1+\beta)\int_0^1\phi_i\,d\overline{x}-\beta\left(\int_0^1\phi_i^2 d\overline{x}\right)q_i\right)\\
&\text{for } i=1, 2, \ldots, n
\end{aligned} \tag{46}$$

with an over dot denoting a derivative with respect to the normalized time $\overline{t}$. Introducing the following variables:

$$q_{i0}=q_i \tag{47a}$$

$$q_{i1}=\dot{q}_i \tag{47b}$$

where $i=1, 2, \ldots, n$, we have:

$$\dot{q}_{i0}=q_{i1} \tag{48a}$$

$$\dot{q}_{i1}=\ddot{q}_i \tag{48b}$$

Further introducing Eqs. (47) and (48b) into Eq. (46), we obtain:

$$\begin{aligned}
&\left(\int_0^1 \phi_i^2 d\overline{x}\right)\dot{q}_{i1}-2\sum_{j=1}^{n}\sum_{k=1}^{n}\left(\int_0^1 \phi_k\phi_j\phi_i\,d\overline{x}\right)q_{k0}\dot{q}_{j1}\\
&+\sum_{j=1}^{n}\sum_{k=1}^{n}\sum_{l=1}^{n}\left(\int_0^1 \phi_l\phi_k\phi_j\phi_i\,d\overline{x}\right)q_{l0}q_{k0}\dot{q}_{j1}\\
&+\overline{c_d}\left(\int_0^1 \phi_i^2 d\overline{x}\right)q_{i1}-2\overline{c_d}\sum_{j=1}^{n}\sum_{k=1}^{n}\left(\int_0^1 \phi_k\phi_j\phi_i\,d\overline{x}\right)q_{k0}q_{j1}\\
&+\overline{c_d}\sum_{j=1}^{n}\sum_{k=1}^{n}\sum_{l=1}^{n}\left(\int_0^1 \phi_l\phi_k\phi_j\phi_i\,d\overline{x}\right)q_{l0}q_{k0}q_{j1}\\
&+\lambda_i^4\left(\int_0^1 \phi_i^2 d\overline{x}\right)q_{i0}-2\sum_{j=1}^{n}\sum_{k=1}^{n}\left(\int_0^1 \phi_k\phi_j\phi_i\,d\overline{x}\right)\lambda_j^4q_{k0}q_{j0}\\
&+\sum_{j=1}^{n}\sum_{k=1}^{n}\sum_{l=1}^{n}\left(\int_0^1 \phi_l\phi_k\phi_j\phi_i\,d\overline{x}\right)\lambda_j^4q_{l0}q_{k0}q_{j0}\\
&-\alpha\left(\sum_{j=1}^{n}\sum_{k=1}^{n}\left(\int_0^1 \phi_k'\phi_j' d\overline{x}\right)q_{k0}q_{j0}\right)\left(\sum_{j=1}^{n}\left(\int_0^1 \phi_j''\phi_i\,d\overline{x}\right)q_{j0}\right.\\
&-2\sum_{j=1}^{n}\sum_{k=1}^{n}\left(\int_0^1 \phi_k\phi_j''\phi_i\,d\overline{x}\right)q_{k0}q_{j0}\\
&\left.+\sum_{j=1}^{n}\sum_{k=1}^{n}\sum_{l=1}^{n}\left(\int_0^1 \phi_l\phi_k\phi_j''\phi_i\,d\overline{x}\right)q_{l0}q_{k0}q_{j0}\right)\\
&=\left(\overline{V_{AC}}\cos(\overline{\omega}\overline{t})\right)^2\left((1+\beta)\int_0^1\phi_i\,d\overline{x}-\beta\left(\int_0^1\phi_i^2 d\overline{x}\right)q_{i0}\right)\\
&\text{for } i=1, 2, \ldots, n
\end{aligned} \tag{49}$$

Equations (48a) and (49) are $2n$ first-order differential equations. With the initial deflection and velocity equal to zero ($q_{i0}=q_{i1}=0$ at $\overline{t}=0$), we solve Eqs. (48a) and (49) using the commercial software Matlab. The function ode45 based on an explicit Runge–Kutta method is adopted. To obtain a steady-state solution, we solve the equations over a long period of time, i.e., $\overline{t}=0\sim 2000$, so-called the long-time integration. It is shown in the literature that the reduced-order model using five modes can accurately describe the dynamic behavior of microbeams (Caruntu and Martinez 2014; Ouakad and Younis 2010). Therefore, we take the first five vibration modes in this study, i.e., taking $n=5$ in Eq. (45).

4 Results and discussions

4.1 Effects of applied AC voltage and mid-plane stretching

Let us consider an electrically actuated microbeam system described in Table 2. Two levels of initial gap between the microbeam and the rigid electrode are taken into account in this table, i.e., large gap of 5 μm and small one of 0.5 μm. With the aid of Tables 1 and 2, we obtain the following dimensionless quantities: $\overline{V_{AC}} = 0 \sim 4$ for both large and small gaps, stretching parameter $\alpha = 1.5$ for large gap and 0.015 for small gap. Introducing the values of $\overline{V_{AC}}$ and α into Eq. (41a) and taking the fringing field parameter $\beta = 0$ (no fringing field effect) and quality factor $Q = 1000$ (using Eq. (43) to obtain the dimensionless damping coefficient $\overline{c_d}$), we solve the resulting equation at different levels of the detuning parameter δ, and obtain the frequency response of the microbeam. The typical results are shown in Figs. 2 and 3.

Figure 2 is for the large initial gap of 5 μm, which corresponds to a large stretching parameter of 1.5. It is seen from the figure that the dynamic behavior of the microbeam depends on the normalized AC voltage amplitude $\overline{V_{AC}}$. When $\overline{V_{AC}}$ is small (e.g., 0.2 in Fig. 2a), the linear frequency response is observed with the maximum deflection changing gradually with the frequency of the applied AC voltage. When $\overline{V_{AC}}$ becomes larger (0.6 in Fig. 2b), the microbeam exhibits the frequency response of hardening characteristic. With the increase of the applied frequency, the maximum deflection increases gradually until reaching the first saddle-node bifurcation point *SN1*, where the deflection drops (*SN1* → ① in Fig. 2b). During the decrease of the applied frequency, the maximum deflection increases gradually until the second saddle-node bifurcation point *SN2*, where it jumps (*SN2* → ②). In the remainder of this paper, such a characteristic frequency response associated with the hardening effect on the microbeam will be named "hardening frequency response". When $\overline{V_{AC}}$ is large (e.g., 2 in Fig. 2c), near the primary resonance regime, a transient dimensionless deflection reaching 1 is predicted by the long-time integration. This indicates that the beam deflection equals to the initial gap between the beam and the electrode, so the microbeam has collapsed onto the rigid electrode. Such behavior is called the dynamic pull-in instability.

Reducing the initial gap between the microbeam and the rigid electrode can reduce the actuation voltage for the microbeam. Figure 3 shows the case of a small initial gap of 0.5 μm, which corresponds to a small stretching parameter of 0.015. Different from the case of a large stretching parameter in Fig. 2, the hardening frequency response is not observed in Fig. 3. The microbeam exhibits the linear frequency response at small levels of $\overline{V_{AC}}$, as shown in Figs. 3a, b; while at large levels of $\overline{V_{AC}}$, it exhibits the dynamic pull-in behavior, as shown in Fig. 3c.

It is noted for Figs. 2 and 3 that the results from the analytical model given in Eq. (41a) agree well with those from the numerical simulations using long-time integration, except when there is dynamic pull-in behavior. The analytical model cannot capture the dynamic pull-in (Caruntu and Knecht 2011).

Figures 2 and 3 show that the dynamic behavior of the microbeam highly depends on the normalized AC voltage amplitude $\overline{V_{AC}}$ and the stretching parameter α. To define the levels of $\overline{V_{AC}}$ and α at which

Table 2 Values of the dimensional quantities for an electrically actuated microbeam system

Quantity	Meaning	Value
E	Young's modulus	160 GPa for silicon, given in Zhang et al. (2007)
v	Poisson's ratio	0.27 for silicon, given in Zhang et al. (2007)
g_0	Initial gap between microbeam and rigid electrode	Large gap: 5 μm
		Small gap: 0.5 μm
h	Beam thickness	10 μm
L	Beam length	500 μm
V_{AC}	Amplitude of alternating current voltage	Large gap: 0–320 V
		Small gap: 0–10 V

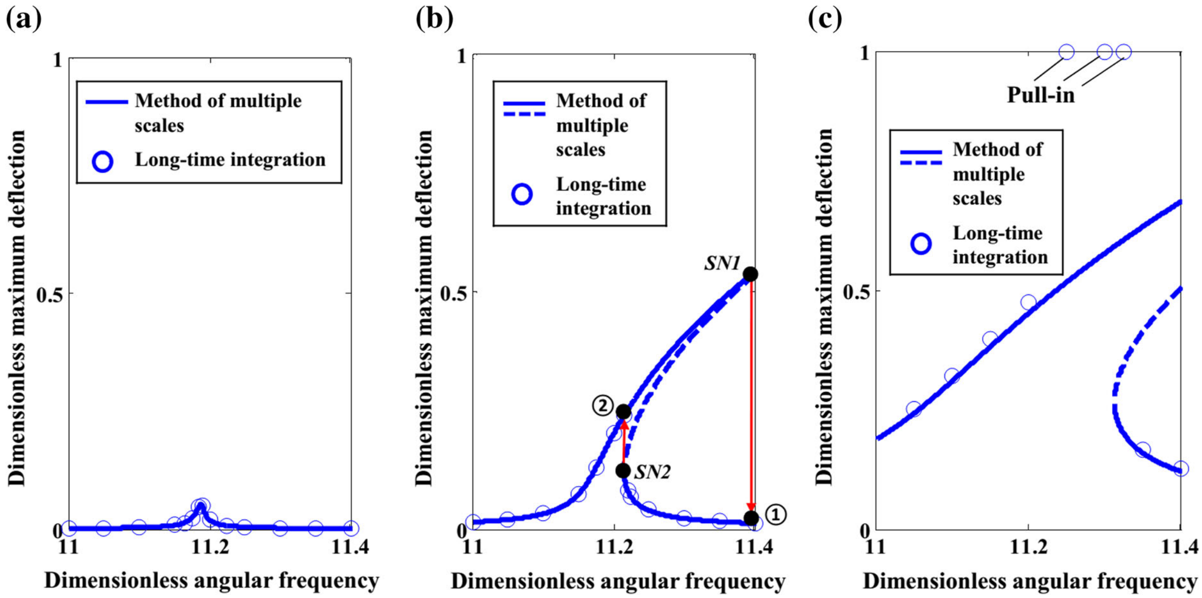

Fig. 2 Frequency response at different levels of AC voltage amplitude: **a** $\overline{V_{AC}} = 0.2$, **b** $\overline{V_{AC}} = 0.6$ and **c** $\overline{V_{AC}} = 2$. Stretching parameter $\alpha = 1.5$. *SN1* and *SN2* are saddle-node bifurcation points. *Solid* and *dashed lines* are respectively the stable and unstable responses

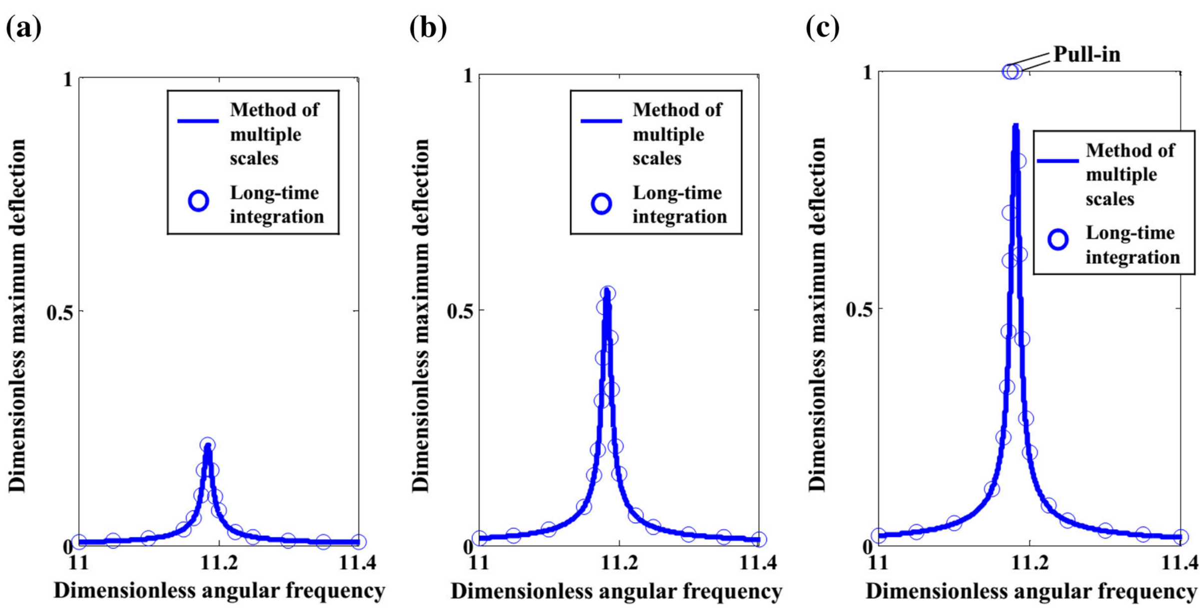

Fig. 3 Frequency response at different levels of AC voltage amplitude: **a** $\overline{V_{AC}} = 0.4$, **b** $\overline{V_{AC}} = 0.6$ and **c** $\overline{V_{AC}} = 0.7$. Stretching parameter $\alpha = 0.015$. *Solid* and *dashed lines* are respectively the stable and unstable responses

the microbeam exhibits the characteristic dynamic behavior, we solve Eq. (41a) at different levels of $\overline{V_{AC}}$ (0–4) and α (0.0006–6) and mark the characteristic feature of the obtained frequency response in a diagram in terms of $\overline{V_{AC}}$ and α, as shown in Fig. 4. The dynamic pull-in behavior is also marked in the figure by the predictions from the long-time integration.

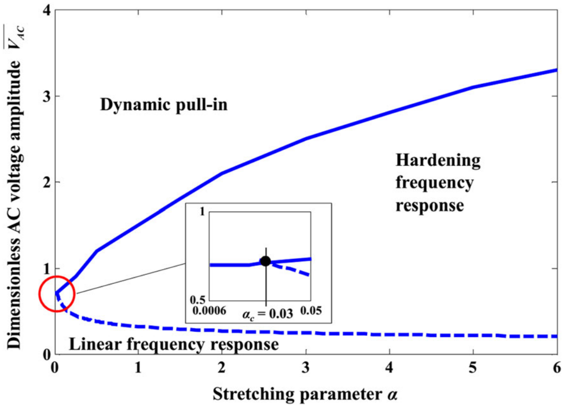

Fig. 4 Design diagram identifying the dynamic behavior of a clamped–clamped microbeam under alternating current voltage. The *inset* shows the minimum allowable stretching parameter $\alpha_c = 0.03$ for the existence of hardening frequency response

Figure 4 shows that when $\overline{V_{AC}}$ is low, the microbeam exhibits the linear frequency response. At low levels of $\overline{V_{AC}}$, the beam deflection is small, and as a result, the mid-plane stretching is insignificant. With the increase of $\overline{V_{AC}}$, the beam deflection increases, and the mid-plane stretching (leading to a hardening effect on the microbeam) becomes more significant. Consequently, the microbeam exhibits a hardening frequency response. At high levels of $\overline{V_{AC}}$, the beam deflection becomes large. So the beam can be close to the rigid electrode. In this case, it may collapse onto the electrode, i.e., dynamic pull-in. On the other hand, high actuating voltage leads to a large electrostatic force, which results in a softening effect on the microbeam (Jia et al. 2012). So the microbeam may also exhibit a frequency response of softening characteristic. However, it is seen from Fig. 4 that the softening frequency response is suppressed and the dynamic pull-in is dominant. This is different from the case of the microbeam biased by a DC voltage. In the case of a DC-biased microbeam, the softening frequency response can be observed at high levels of DC voltage (Mestrom et al. 2008).

The inset of Fig. 4 also shows that the stretching parameter α should be large enough for the existence of the hardening frequency response. In fact, α quantifies the effect of mid-plane stretching; i.e., by increasing α, the mid-plane stretching becomes more significant, which leads to the stiffening of the microbeam. The expression in Table 1 indicates that in order to control α, we can adjust the beam thickness h and/or the initial gap g_0 between the beam and the electrode.

4.2 Effects of fringing field and damping

The fringing field effect due to the finite size of the beam width b is described by a fringing field parameter β, whose expression can be found from Table 1 as $0.65g_0/b$ with g_0 being the initial gap between the beam and the rigid electrode. For the proper application of Palmer's formula to estimate the electrostatic force, the microbeam system must satisfy the inequality $b > 10g_0$ (Caruntu and Knecht 2011). In this case,

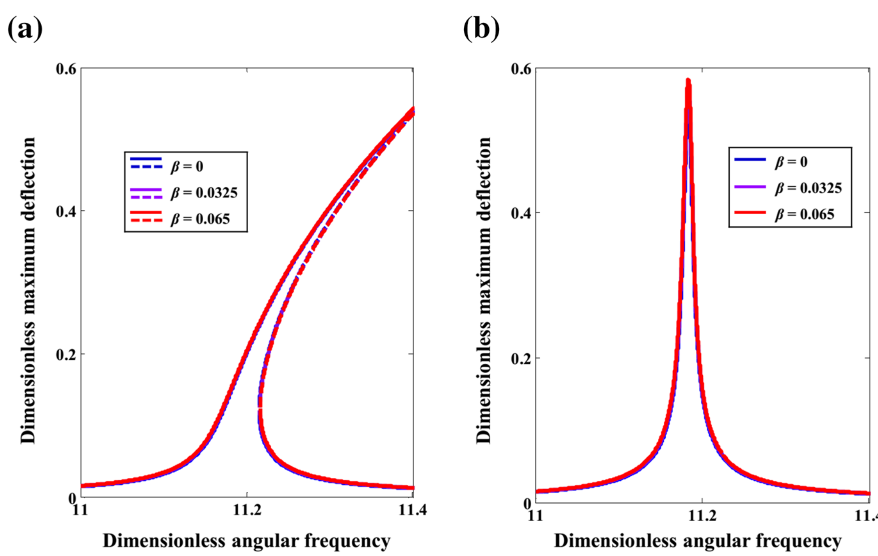

Fig. 5 Frequency response at different levels of fringing field parameter β: **a** for stretching parameter $\alpha = 1.5$ and **b** for $\alpha = 0.015$. In both figures, $\overline{V_{AC}} = 0.6$, quality factor $Q = 1000$. *Solid* and *dashed lines* are respectively the stable and unstable responses

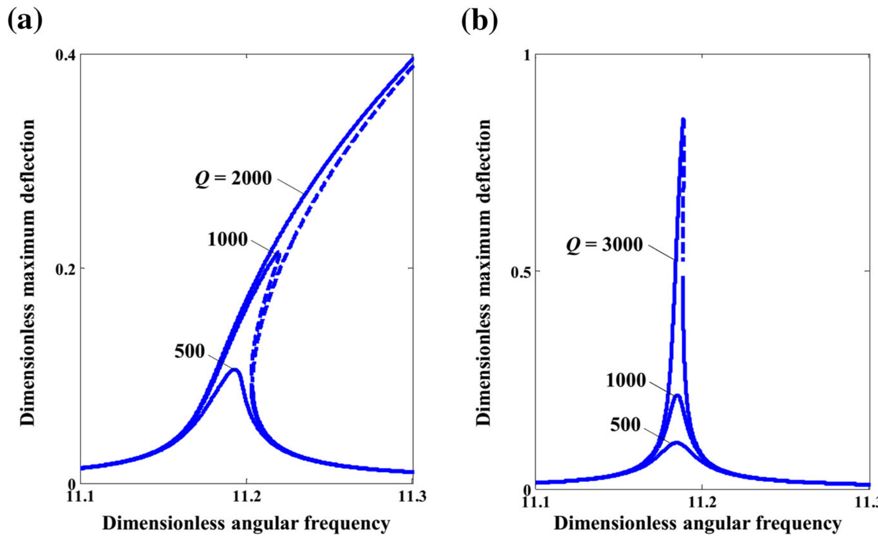

Fig. 6 Frequency response at different levels of quality factor Q: **a** for stretching parameter $\alpha = 1.5$ and **b** for $\alpha = 0.015$. In both figures, $\overline{V_{AC}} = 0.4$, fringing field parameter $\beta = 0$ (no fringing field effect). *Solid* and *dashed lines* are respectively the stable and unstable responses

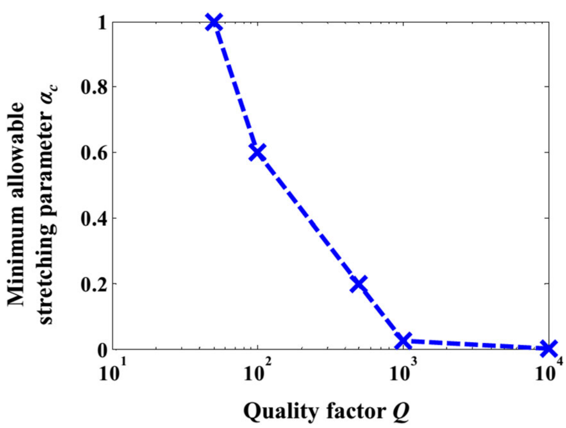

Fig. 7 Minimum allowable stretching parameter α_c for the existence of hardening frequency response: effect of quality factor Q

β varies between 0 and 0.065. Using Eqs. (41a) and (43) with Tables 1 and 2, we obtain the frequency responses at different levels of β (0–0.065), as depicted in Fig. 5. It is seen from the figure that the effect of β at the studied level is negligible.

The frequency responses of the microbeam at different levels of quality factor Q are shown in Fig. 6. To obtain this figure, Tables 1 and 2 and Eqs. (41a) and (43) are used. Figure 6a indicates that increasing Q strengthens the hardening effect. Q is inversely proportional to the dimensionless damping coefficient $\overline{c_d}$ (see Eq. (43)). So increasing Q reduces the damping effect ($\overline{c_d}$ decreases), which results in an increase of the beam deflection. Therefore, the hardening effect due to mid-plane stretching becomes more significant. Figure 6b further indicates that Q influences the minimum allowable stretching parameter for the existence of hardening frequency response: when $Q = 1000$, the stretching parameter α should be larger than 0.03 to observe the hardening frequency response (refer to Fig. 4); however, when $Q = 3000$, hardening frequency response is observed at $\alpha = 0.015$ (<0.03) in Fig. 6b. Using the analytical model (Eq. (41a) and the long-time integration presented in Sect. 3.2, we obtain the minimum allowable stretching parameter α_c at different levels of quality factor Q, as shown in Fig. 7. Increasing Q strengthens the hardening effect, so α_c decreases with the increase of Q.

4.3 Effects of boundary conditions

The microbeam investigated in the previous Sects. 4.1 and 4.2 is clamped at both ends. The beam can also be subjected to other boundary conditions such as simply-supported and cantilever, as shown in Fig. 8. This subsection is devoted to studying the effects of boundary conditions on the dynamic behavior of the microbeam.

Figure 8a shows a simply-supported microbeam. Its axial displacements at the two beam ends are the same as those of the clamped–clamped beam, i.e.,

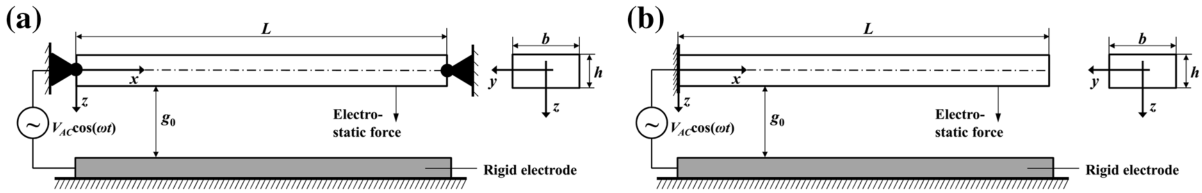

Fig. 8 Microbeam under different boundary conditions: **a** simply-supported and **b** cantilever

$u(0) = u(L) = 0$. Therefore, the axial force expressed in Eq. (16) for the clamped–clamped beam can also be used for the simply-supported beam. As a result, the same governing equation Eq. (18) can be used. By taking the first linear undamped vibration mode ϕ_1 of simply-supported beam:

$$\phi_1(\overline{x}) = \sin(\pi\overline{x}) \tag{50}$$

with the frequency parameter $\lambda_1 = \pi$, and following the similar procedure to the one adopted in Sect. 3.1, we obtain the same expression as Eq. (41a) to study the frequency response of the simply-supported beam.

A cantilever-type microbeam anchored at one end is shown in Fig. 8b. The axial force at the free end of the beam is zero, i.e., $N(L,t) = 0$. Then from Eq. (12a) we have:

$$N(x,t) = 0 \tag{51}$$

With Eqs. (51) and (15b), Eq. (13) can be reduced to:

$$\begin{aligned} &\rho S\frac{\partial^2 w}{\partial t^2} + c_d\frac{\partial w}{\partial t} + E^* I\frac{\partial^4 w}{\partial x^4} \\ &\quad = \frac{1}{2}\frac{\varepsilon_0 b (V_{AC}\cos(\omega t))^2}{(g_0 - w)^2}\left(1 + 0.65\frac{g_0 - w}{b}\right) \end{aligned} \tag{52}$$

Introducing the quantities in Table 1, we rewrite Eq. (52) in the following dimensionless form:

$$\begin{aligned} &\frac{\partial^2 \overline{w}}{\partial \overline{t}^2} + \overline{c_d}\frac{\partial \overline{w}}{\partial \overline{t}} + \frac{\partial^4 \overline{w}}{\partial \overline{x}^4} \\ &\quad = \left(\overline{V_{AC}}\cos(\overline{\omega}\overline{t})\right)^2\left(\frac{1}{(1-\overline{w})^2} + \frac{\beta}{(1-\overline{w})}\right) \end{aligned} \tag{53}$$

The mid-plane stretching term does not exist in Eq. (53) because there is no axial force in the cantilever (refer to Eq. (51)). Therefore, the cantilever-type microbeam cannot exhibit the hardening frequency response. Taking the first linear undamped vibration mode ϕ_1 of cantilever:

$$\phi_1(\overline{x}) = C_1\left(\cosh(\lambda_1\overline{x}) - \cos(\lambda_1\overline{x}) - \frac{\sinh(\lambda_1) - \sin(\lambda_1)}{\cosh(\lambda_1) + \cos(\lambda_1)}(\sinh(\lambda_1\overline{x}) - \sin(\lambda_1\overline{x}))\right) \tag{54}$$

with C_1 satisfying $\max\limits_{\overline{x}\in[0,1]}|\phi_1(\overline{x})| = 1$ and λ_1 satisfying $\cosh(\lambda_1)\cos(\lambda_1) = -1$, and following the procedures in Sect. 3.1, we obtain a similar expression to

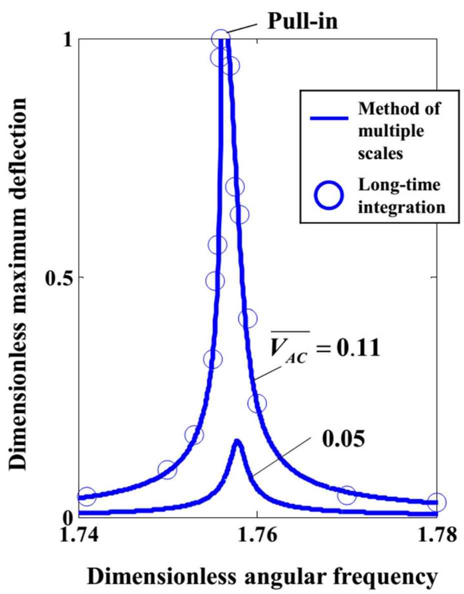

Fig. 9 Frequency response of cantilever-type microbeam at different levels of AC voltage amplitude

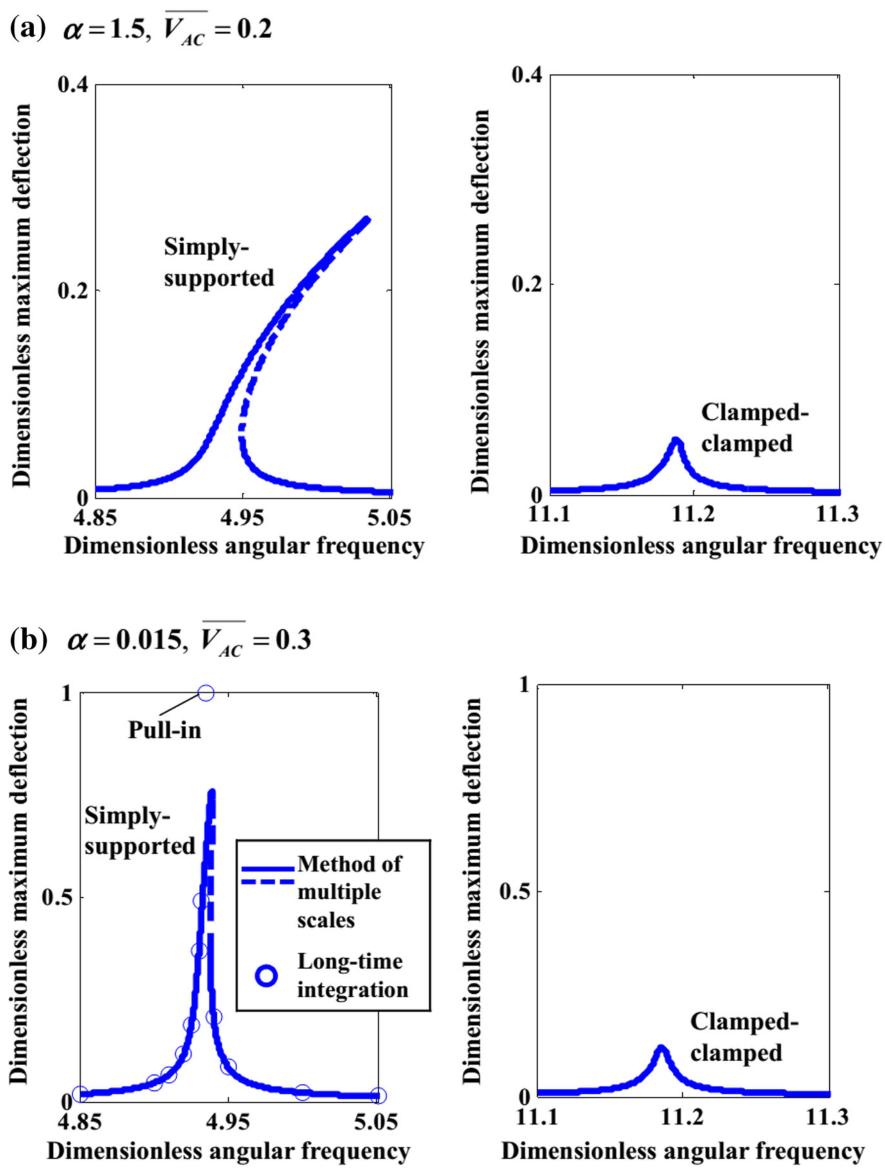

Fig. 10 Frequency response of simply-supported and clamped–clamped microbeams: **a** for $\alpha = 1.5$, $\overline{V_{AC}} = 0.2$ and **b** for $\alpha = 0.015$, $\overline{V_{AC}} = 0.3$. *Solid* and *dashed lines* are respectively the stable and unstable responses

Eq. (41a). The only difference is that the coefficient b_3 in Eq. (41a) is modified to be $\frac{3m_4}{8m_2\omega_1}(4+\beta)\overline{V_{AC}}^2$.

Using Tables 1 and 2 and Eqs. (41a) and (43), and taking the fringing field parameter $\beta = 0$, quality factor $Q = 1000$, we obtain the frequency responses of the microbeam under different boundary conditions. The results of the cantilever-type microbeam are depicted in Fig. 9. As predicted, the cantilever cannot exhibit the hardening frequency response. At low levels of $\overline{V_{AC}}$, the linear frequency response is observed (see $\overline{V_{AC}} = 0.05$ in Fig. 9); while at high levels (e.g., $\overline{V_{AC}} = 0.11$), the dynamic pull-in near the primary resonance frequency is predicted by the long-time integration.

The frequency responses of simply-supported and clamped–clamped microbeams are compared in Fig. 10. It is found from Fig. 10a that the hardening effect in the simply-supported beam is more significant than that in the clamped–clamped beam. Moreover, Fig. 10b shows that compared with the clamped–

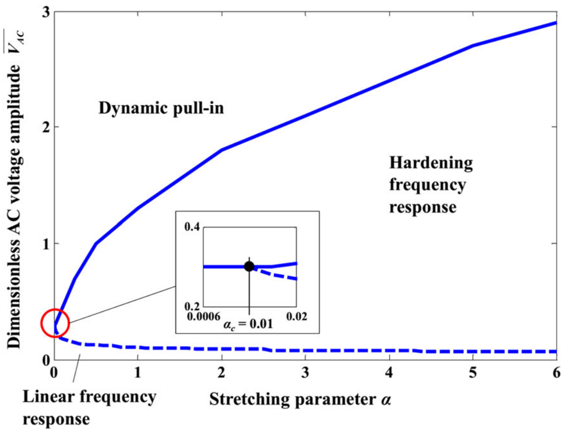

Fig. 11 Design diagram identifying the dynamic behavior of an electrically actuated simply-supported microbeam. The *inset* depicts the minimum allowable stretching parameter $\alpha_c = 0.01$ for the existence of hardening frequency response

clamped beam, the simply-supported one is prone to pull-in. The reduced rotation at the two ends of the clamped–clamped microbeam makes it more difficult to bend, and as a result, the dynamic pull-in is hindered. The beam deflection is also reduced, which weakens the hardening effect due to mid-plane stretching.

Using Tables 1 and 2, Eq. (41a), and the long-time integration in Sect. 3.2, we draw the design diagram for the simply-supported microbeam in Fig. 11. The figure is analogous to Fig. 4 of the clamped–clamped microbeam. However, smaller voltage input $\overline{V_{AC}}$ is required to induce the dynamic pull-in and the hardening frequency response in the simply-supported beam. Moreover, the insets in Figs. 4 and 11 show that the simply-supported beam has a smaller minimum allowable stretching parameter α_c for the existence of hardening frequency response. The stiffer fixation as observed in the clamped–clamped fixation versus the simply-supported case weakens the hardening effect and makes it more difficult to actuate the beam. Consequently, higher α_c (stronger hardening effect) and higher $\overline{V_{AC}}$ (larger electrostatic force) are needed for the clamped–clamped beam.

5 Conclusions

The dynamic behavior of a microbeam under various levels of AC (alternating current) voltage is investigated. The beam model is developed using Euler–Bernoulli beam theory. The mid-plane stretching, fringing field and damping effects are all taken into account in the model formulation. The transient response and the steady-state frequency response of the microbeam under different boundary conditions are derived from the beam model respectively by the method of multiple scales and the long-time integration.

Our results reveal that unlike the microbeam biased by a DC voltage, the non-biased microbeam does not exhibit the softening frequency response. Our results also reveal that the characteristic feature of the dynamic behavior of the non-biased microbeam highly depends on the applied AC voltage and the mid-plane stretching parameter α, which can be altered by the beam thickness and the initial gap between the beam and the rigid electrode. A diagram in terms of α and AC voltage amplitude is developed to show the domains of characteristic dynamic behaviors. The diagram provides some basic guidelines for designing the micro-resonators. Furthermore, our results real that damping and boundary conditions have significant effects on the dynamic behavior of the microbeam, while the effect of fringing field is negligible.

Acknowledgments The financial support provided by the Natural Sciences and Engineering Research Council of Canada and the Discovery Accelerator Supplements is gratefully acknowledged.

References

Almog, R., Zaitsev, S., Shtempluck, O., Buks, E.: Noise squeezing in a nanomechanical duffing resonator. Phys. Rev. Lett. **98**, 078103 (2007)

Alsaleem, F.M., Younis, M.I., Ouakad, H.M.: On the nonlinear resonances and dynamic pull-in of electrostatically actuated resonators. J. Micromech. Microeng. **19**, 045013 (2009)

Badzey, R.L., Zolfagharkhani, G., Gaidarzhy, A., Mohanty, P.: A controllable nanomechanical memory element. Appl. Phys. Lett. **85**, 3587–3589 (2004)

Batra, R.C., Porfiri, M., Spinello, D.: Electromechanical model of electrically actuated narrow microbeams. J. Microelectromech. S. **15**, 1175–1189 (2006)

Brown, E.R.: RF-MEMS switches for reconfigurable integrated circuits. IEEE T. Microw. Theory **46**, 1868–1880 (1998)

Burg, T.P., Godin, M., Knudsen, S.M., Shen, W., Carlson, G., Foster, J.S., Babcock, K., Manalis, S.R.: Weighing of biomolecules, single cells and single nanoparticles in fluid. Nature **446**, 1066–1069 (2007)

Carr, D.W., Evoy, S., Sekaric, L., Craighead, H.G., Parpia, J.M.: Measurement of mechanical resonance and losses in nanometer scale silicon wires. Appl. Phys. Lett. **75**, 920–922 (1999)

Caruntu, D.I., Knecht, M.W.: On nonlinear response near-half natural frequency of electrostatically actuated microresonators. Int. J. Struct. Stab. Dyn. **11**, 641–672 (2011)

Caruntu, D.I., Martinez, I.: Reduced order model of parametric resonance of electrostatically actuated MEMS cantilever resonators. Int. J. Nonlinear Mech. **66**, 28–32 (2014)

Caruntu, D.I., Martinez, I., Knecht, M.W.: Reduced order model analysis of frequency response of alternating current near half natural frequency electrostatically actuated MEMS cantilevers. J. Comput. Nonlinear Dyn. **8**, 031011 (2013)

Charlot, B., Sun, W., Yamashita, K., Fujita, H., Toshiyoshi, H.: Bistable nanowire for micromechanical memory. J. Micromech. Microeng. **18**, 045005 (2008)

Chaste, J., Eichler, A., Moser, J., Ceballos, G., Rurali, R., Bachtold, A.: A nanomechanical mass sensor with yoctogram resolution. Nat. Nanotech. **7**, 301–304 (2012)

Chiu, H.-Y., Hung, P., Postma, H.W.Ch., Bockrath, M.: Atomic-scale mass sensing using carbon nanotube resonators. Nano Lett. **8**, 4342–4346 (2008)

Eltaher, M.A., Agwa, M.A., Mahmoud, F.F.: Nanobeam sensor for measuring a zeptogram mass. Int. J. Mech. Mater. Des. **12**, 211–221 (2016)

Evoy, S., Carr, D.W., Sekaric, L., Olkhovets, A., Parpia, J.M., Craighead, H.G.: Nanofabrication and electrostatic operation of single-crystal silicon paddle oscillators. J. Appl. Phys. **86**, 6072–6077 (1999)

Farokhi, H., Ghayesh, M.H.: Size-dependent behaviour of electrically actuated microcantilever-based MEMS. Int. J. Mech. Mater. Des. (2015a). doi:10.1007/s10999-015-9295-0

Farokhi, H., Ghayesh, M.H.: Nonlinear resonant response of imperfect extensible Timoshenko microbeams. Int. J. Mech. Mater. Des. (2015b). doi:10.1007/s10999-015-9316-z

Gui, C., Legtenberg, R., Tilmans, H.A.C., Fluitman, J.H.J., Elwenspoek, M.: Nonlinearity and hysteresis of resonant strain gauges. J. Microelectromech. Syst. **7**, 122–127 (1998)

Gupta, R.K.: Electrostatic pull-in test structure design for in situ mechanical property measurements of microelectromechanical systems (MEMS). Ph.D. thesis, Massachusetts Institute of Technology, USA (1997)

Hopcroft, M.A., Kim, B., Chandorkar, S., Melamud, R., Agarwal, M., Jha, C.M., Bahl, G., Salvia, J., Mehta, H., Lee, H.K., Candler, R.N., Kenny, T.W.: Using the temperature dependence of resonator quality factor as a thermometer. Appl. Phys. Lett. **91**, 013505 (2007)

Intaraprasonk, V., Fan, S.: Nonvolatile bistable all-optical switch from mechanical buckling. Appl. Phys. Lett. **98**, 241104 (2011)

Jang, J.E., Cha, S.N., Choi, Y.J., Kang, D.J., Butler, T.P., Hasko, D.G., Jung, J.E., Kim, J.M., Amaratunga, G.A.J.: Nanoscale memory cell based on a nanoelectromechanical switched capacitor. Nat. Nanotech. **3**, 26–30 (2008)

Jia, X.L., Yang, J., Kitipornchai, S., Lim, C.W.: Resonance frequency response of geometrically nonlinear micro-switches under electrical actuation. J. Sound Vib. **331**, 3397–3411 (2012)

Jonsson, L.M., Axelsson, S., Nord, T., Viefers, S., Kinaret, J.M.: High frequency properties of a CNT-based nanorelay. Nanotechnology **15**, 1497–1502 (2004)

Kacem, N., Baguet, S., Hentz, S., Dufour, R.: Computational and quasi-analytical models for non-linear vibrations of resonant MEMS and NEMS sensors. Int. J. Nonlinear Mech. **46**, 532–542 (2011)

Kim, I.K., Lee, S.I.: Theoretical investigation of nonlinear resonances in a carbon nanotube cantilever with a tip-mass under electrostatic excitation. J. Appl. Phys. **114**, 104303 (2013)

Kivi, A.R., Azizi, S., Khalkhali, A.: Sensitivity enhancement of a MEMS sensor in nonlinear regime. Int. J. Mech. Mater. Des. (2015). doi:10.1007/s10999-015-9310-5

Kuang, J.-H., Chen, C.-J.: Dynamic characteristics of shaped micro-actuators solved using the differential quadrature method. J. Micromech. Microeng. **14**, 647–655 (2004)

Kwon, T., Eom, K., Park, J., Yoon, D.S., Lee, H.L., Kim, T.S.: Micromechanical observation of the kinetics of biomolecular interactions. Appl. Phys. Lett. **93**, 173901 (2008)

Mestrom, R.M.C., Fey, R.H.B., van Beek, J.T.M., Phan, K.L., Nijmeijer, H.: Modelling the dynamics of a MEMS resonator: simulations and experiments. Sens. Actuators A **142**, 306–315 (2008)

Mohanty, P.: Nano-oscillators get it together. Nature **437**, 325–326 (2005)

Nayfeh, A.H., Younis, M.I., Abdel-Rahman, E.M.: Dynamic pull-in phenomenon in MEMS resonantors. Nonlinear Dyn. **48**, 153–163 (2007)

Ouakad, H.M., Younis, M.I.: The dynamic behavior of MEMS arch resonators actuated electrically. Int. J. Nonlinear Mech. **45**, 704–713 (2010)

Palmer, H.B.: The capacitance of a parallel-plate capacitor by the Schwartz-Christoffel transformation. Trans. Am. Inst. Elect. Eng. **56**, 363–366 (1937)

Peng, H.B., Chang, C.W., Aloni, S., Yuzvinsky, T.D., Zettl, A.: Ultrahigh frequency nanotube resonators. Phys. Rev. Lett. **97**, 087203 (2006)

Reddy, J.N.: Microstructure-dependent couple stress theories of functionally graded beams. J. Mech. Phys. Solids **59**, 2382–2399 (2011)

Rhoads, J.F., Shaw, S.W., Turner, K.L.: The nonlinear response of resonant microbeam systems with purely-parametric electrostatic actuation. J. Micromech. Microeng. **16**, 890–899 (2006)

Roodenburg, D., Spronck, J.W., van der Zant, H.S.J., Venstra, W.J.: Buckling beam micromechanical memory with on-chip readout. Appl. Phys. Lett. **94**, 183501 (2009)

Rueckes, T., Kim, K., Joselevich, E., Tseng, G.Y., Cheung, C.-L., Lieber, C.M.: Carbon nanotube—based nonvolatile random access memory for molecular computing. Science **289**, 94–97 (2000)

Ruzziconi, L., Bataineh, A.M., Younis, M.I., Cui, W., Lenci, S.: Nonlinear dynamics of an electrically actuated imperfect microbeam resonator: experimental investigation and reduced-order modeling. J. Micromech. Microeng. **23**, 075012 (2013)

Southworth, D.R., Bellan, L.M., Linzon, Y., Craighead, H.G., Parpia, J.M.: Stress-based vapor sensing using resonant microbridges. Appl. Phys. Lett. **96**, 163503 (2010)

Tilmans, H.A.C., Legtenberg, R.: Electrostatically driven vacuum-encapsulated polysilicon resonators Part II. Theory and performance. Sens. Actuators A **45**, 67–84 (1994)

van der Meijs, N.P., Fokkema, J.T.: VLSI circuit reconstruction from mask topology. Integr. VLSI J. **2**, 85–119 (1984)

Wang, Q., Arash, B.: A review on applications of carbon nanotubes and graphenes as nano-resonator sensors. Comput. Mater. Sci. **82**, 350–360 (2014)

Yang, Y.T., Callegari, C., Feng, X.L., Ekinci, K.L., Roukes, M.L.: Zeptogram-scale nanomechanical mass sensing. Nano Lett. **6**, 583–586 (2006)

Zhang, Y., Wang, Y., Li, Z., Huang, Y., Li, D.: Snap-through and pull-in instabilities of an arch-shaped beam under an electrostatic loading. J. Microelectromech. Syst. **16**, 684–693 (2007)

Zook, J.D., Burns, D.W., Guckel, H., Sniegowski, J.J., Engelstad, R.L., Feng, Z.: Characteristics of polysilicon resonant microbeams. Sens. Actuators A **35**, 51–59 (1992)